



# Hyperspectral Remote Sensing with the UAS “Stuttgarter Adler” – System Setup, Calibration and First Results

AXEL BÜTTNER & HANS-PETER RÖSER, Stuttgart

**Keywords:** hyperspectral, remote sensing, unmanned aerial system, direct georeferencing, calibration

**Summary:** The UAS “Stuttgarter Adler” was designed as a flexible and cost-effective remote-sensing platform for acquisition of high quality environmental data. Different missions for precision agriculture applications and BRDF-research have been successfully performed with a multispectral camera system and a spectrometer as main payloads. Currently, an imaging spectrometer is integrated in the UAS as a new payload, which enables the recording of hyperspectral data in more than 200 spectral bands in the visible and near infrared spectrum. The recording principle of the hyperspectral instrument is based on a pushbroom line scanner. Each line is stored as a matrix image with spectral information in one axis and spatial information in the other axis of the image. Besides a detailed specification of the system concept and instrument design, the calibration procedure of the hyperspectral sensor system is discussed and results of the laboratory calibration are presented. The complete processing chain of measurement data is described and first preliminary results of measurement-flights over agricultural test sites are presented.

**Zusammenfassung:** *Hyperspektrale Fernerkundung mit dem UAS „Stuttgarter Adler“ – Systemübersicht, Kalibrierung und erste Ergebnisse.* Am Institut für Raumfahrtssysteme (IRS) der Universität Stuttgart wurde in den letzten Jahren das UAS „Stuttgarter Adler“ als flexible Fernerkundungsplattform entwickelt und erfolgreich zur multispektralen Fernerkundung sowie für BRDF-Messungen eingesetzt. Aktuell befindet sich als neue Nutzlast ein abbildendes Spektrometer in der Erprobung. Dieses ermöglicht die Aufzeichnung von hyperspektralen Daten in über 200 Bändern im sichtbaren und nahen infraroten Spektralbereich. In diesem Beitrag wird die Integration und Inbetriebnahme des hyperspektralen Sensors als neue Nutzlast erläutert. Dabei werden neben einer detaillierten Beschreibung des Sensorsystems auf dessen radiometrische und spektrale Kalibrierung sowie das Prozessieren der Daten eingegangen und erste Erfahrungen und Ergebnisse des Systems im Einsatz diskutiert.

## 1 Introduction

Hyperspectral remote sensing data is of great interest in many different research topics and applications. It combines traditional 2D imaging remote sensing technology with classical spectroscopy and allows the acquisition of data with both, geometric and spectral high resolution. The large number of spectral bands provides the ability to derive biophysical and biochemical parameters from the quasi continuous visible and near infrared spectrum

(HABOUDANE et al. 2008), while the geometric resolution can be used for the creation of rectified image strips. In the last decades, hyperspectral remote sensing was mainly performed with airborne sensors such as AVIRIS or HyMap, which are employed on manned aircraft (GREEN et al. 1998, COCKS et al. 1998). The development of compact and lightweight imaging spectrometers in the last few years offers the possibility to integrate such instruments in small unmanned aerial systems (UAS) and closes the gap between time-con-

suming and spatially limited point measurements on the ground and complex and expensive flight campaigns with manned aircraft. Recent studies have investigated the integration of a hyperspectral pushbroom sensor in an UAS (HRUSKA et al. 2012) and shown the potentials of such a system for vegetation monitoring and water stress detection (e.g. BERNI et al. 2009, ZARCO-TEJADA et al. 2012, 2013). The UAS “Stuttgarter Adler” is operated as a remote sensing platform at the Institute of Space Systems and can be equipped with different sensor systems like multispectral and thermal cameras (KIRCHGAESSNER 2013). This paper shows the integration of an imaging spectrometer as hyperspectral payload in our UAS, including a detailed description of the system design and calibration concept of the instrument. Results of the laboratory calibration are presented and first results of measurement flights are discussed. A new approach for improving geometric correction and direct georeferencing is introduced.

## 2 System Overview

### 2.1 UAS “Stuttgarter Adler”

The UAS “Stuttgarter Adler” is a remote sensing platform, which was specially designed for acquiring high quality remote sensing data with great flexibility at comparatively low costs (PUTZE 2013). The twin-engine configuration with two 2.0 kW electrical engines has a wing-span of 4.33 m and allows a take-off weight of 25 kg including a payload capacity of 4 kg – 5 kg. The aerodynamic design ac-

**Tab. 1:** Technical data of the UAS.

Wing span	4.33 m
Total length	2.6 m
Max. take-off weight	25 kg
Electric Propulsion	2 x Polytec C42-60 2kW
Batteries	2x 10s2p 8000mAh LiPo
Payload capacity	4 kg – 5 kg
Flight Time	25 min – 30 min



**Fig. 1:** UAS “Stuttgarter Adler” before take-off.

counts for a stable flight at 12 m/s – 15 m/s airspeed. The radio link and all control surfaces are constructed in a redundant way so that no single point failure leads to loss of the aircraft. The integration of the motors in two nacelles provides enough space for the integration of the payload in the fuselage. Take-off and landing require a paved or grass runway of 150 m length and are performed manually with remote control. The flight itself is controlled autonomously by an autopilot system based on the open source project “paparazzi” (BRISSET 2006). The LiPo batteries allow a total flight-time of up to 30 minutes. An image of the UAS is shown in (Fig. 1) and the technical data are summarized in (Tab. 1).

### 2.2 Hyperspectral Sensor System

The hyperspectral imager consists of three main components, see (Fig. 2) (SPECTRAL IMAGING LTD. 2008). Incoming light is focused on the entrance-slit of the spectrograph by a special fore-lens (OLE9 forelens); a monochrome CCD-camera (Prosilica GE1900) is mounted on the back of the spectrograph to detect the radiance; the spectrograph itself (Specim Inspector V10E) disperses the light and focuses it on the CCD detector surface with a nominal spectral resolution of 2.8 nm. The 9 mm lens leads to a maximum field of view of 76.5° which is used for bidirectional reflectance distribution function (BRDF) research in combination with a BRDF ground measurements device (SCHWARZBACH 2012). Nominal measure-

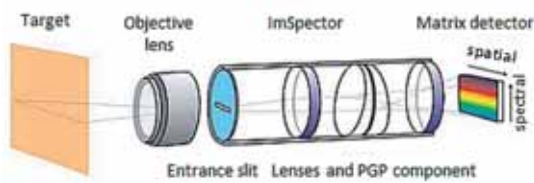


**Fig. 2:** Schematic of the imaging spectrograph.

ments are performed with  $60^\circ$  limited field of view (FOV) to reduce BRDF-effects. The main specifications of the spectrograph are summarized in (Tab. 2).

The hyperspectral imager is working as a pushbroom line scanner with the entrance slit oriented perpendicular to the flight direction. The constant movement of the UAS is used to scan an area in continuous strips. Each single line is stored as a matrix image, which contains spectral information in one dimension and spatial information in the other dimension of the image sensor. The geometric rectification of the image strips is a big challenge in operating a line scanner in an UAS. The small platform is susceptible to gusts of wind and much more unstable in comparison to large

manned aircraft. For correct alignment and rectification of the recorded lines, the position and attitude of the sensor must be known with high precision. Therefore, additional sensors for position and attitude determination are mounted on the spectrograph. To meet the requirements of small and light-weight components for the integration in the UAS, a position and attitude sensor system based on a three-axis micro-electromechanical system (MEMS) accelerometer, gyroscope and magnetometer in combination with a compact L1-GPS receiver providing carrier phase raw measurement data was chosen. A second stationary GPS receiver is used for differential processing against a base station. Barometer and thermometer as additional sensors were added for improving the height determination. The gyroscope used is an ITG-3200 triple-axes gyroscope from InvenSense providing three integrated 16-bit analog-to-digital converters (ADCs) for simultaneous sampling of the gyros. The accelerometer is an Analog Devices ADXL345 digital triaxial acceleration sensor with measurement range up to  $\pm 16$  g, which was designed for low power consumer market. The 13-bit resolution enables measurement of inclination changes smaller than  $0.5^\circ$ . The Honeywell HMC5883L triple-axes sensor is used as digital compass in the hardware setup. The 12-bit ADC enables measurements with milligauss resolution, which lead to a heading accuracy of  $1^\circ$ . An external professional grade global navigation satellite system (GNSS) antenna from Tallysman (TW 2410) is used for acquiring strong GPS signal and improved multipath rejection. The inertial data is recorded with 100 Hz, while the GPS receiver provides raw data with 20 Hz update rate. A small microprocessor board is used for synchronous sensor readout via fast-mode i2c digital interface, a precise GPS pulse-per-second time-signal serves as common time basis. Since no real-time capability is required, a specially designed extended Kalman filter with smoothing techniques is used for sensor fusion of inertial measurement unit (IMU) and GPS data in the post-processing to improve the overall accuracy (KOERNER 2012). The information flow of the tightly coupled filter is shown in (Fig. 3).

**Tab. 2:** Specification of the hyperspectral imager.

<b>Spectrograph</b>	
Spectral range	380 nm – 1100 nm
Spectral resolution	2.8 nm
Numerical aperture	F / 2.4
Slit width	30 $\mu$ m
Spatial resolution	rms spot radius < 9 $\mu$ m
<b>CCD camera and forelens</b>	
Resolution	1920 x 1080
Binning h/v	1–8 pixels / rows
Pixel Size	7.4 $\mu$ m x 7.4 $\mu$ m
Radiometric resolution	12 bit
Frame rate (full resolution)	up to 30 fps
Frame rate (2x binning)	up to 60 fps
Focal length	9 mm
Field of view (max.)	76.5° x 0.19°

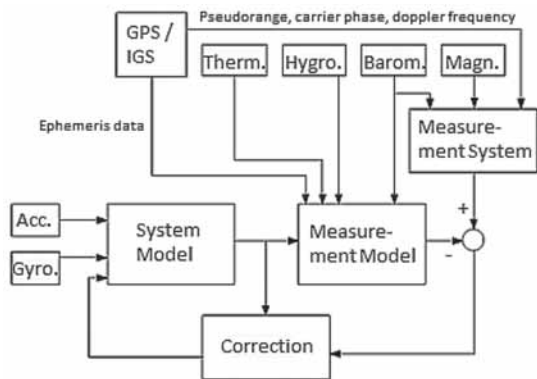


**Fig. 3:** Information flow of the extended Kalman filter.

The whole sensor system is fixed horizontally on a common mounting plate. An optical mirror reflects the incoming light to the fore-lens. Expanded polypropylene-foam is used for vibration isolation from the aircraft. The IMU is mounted directly on top of the spectrometer to keep the position and orientation offset as constant and small as possible. The GPS-antenna is mounted on top of the aircraft right above the instrument for best reception of the GPS satellite signals. A compact PC with Linux operating system, Gigabit-Ethernet interface and solid-state disk for data storage is used as on-board payload computer. Custom software for configuration of the camera and recording of the image data was developed, which enables flexible adjustments of different sensor parameters such as frame rate, binning and exposure time for particular missions.

### 3 Calibration Concept and Data Processing

Radiometric and spectral calibration is performed in-house in an optical laboratory. Different calibration equipment such as an integrating sphere, line emission lamps and a monochromator are available for regular calibration in the laboratory between measurement campaigns. The whole system including mounting plate and mirror is calibrated together to account for possible distortions of the additional components. The results of the

laboratory calibration are used for radiometric pre-processing after measurement flights.

#### 3.1 Radiometric Calibration

The main task of radiometric calibration is the determination of the coefficients for the conversion of raw data (DN) into physical units (spectral radiance,  $\text{mW} / (\text{m}^2 \cdot \text{sr} \cdot \text{nm})$ ). In addition, vignetting effects and sensor inhomogeneities due to slightly varying sensitivities of the CCD elements are corrected. An integrating sphere, which is regularly calibrated against the German national standard (PTB), is used as homogeneous light-source with known spectral radiance. It has a diameter of 500 mm with an output port diameter of 100 mm and is illuminated with a 50 W QTH lamp. The calibration is valid for the spectral range from 380 nm to 1100 nm with a relative uncertainty of 5%. For the determination of the sensor linearity, the integrating sphere is equipped with an adjustable slit in front of the QTH lamp and an optometer for measuring the total radiance. The linearity of the radiometric response function is measured by increasing the luminosity up to saturation level at different integration times. Results show deviations from the linear model to be smaller than 1%, so a linear model is assumed. Dark signal is quantified in the laboratory for different temperatures and integration times to characterize the dark signal non uniformity (DSNU). Noise equivalent spectral radiance (NESR) is determined by measuring the stan-

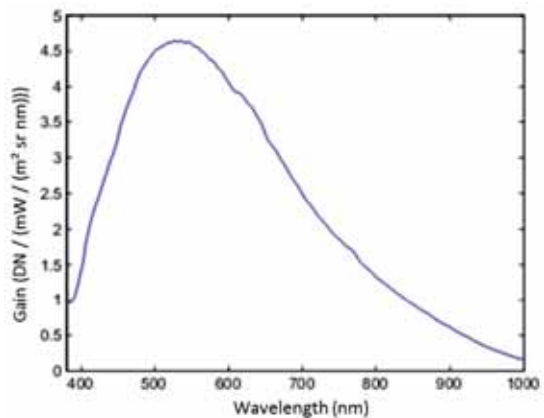


**Fig. 4:** Radiometric calibration coefficient.

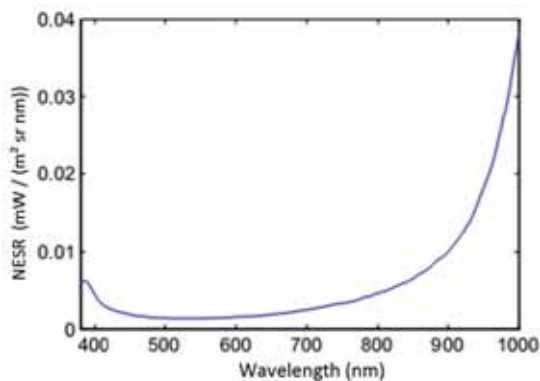


**Fig. 5:** Noise equivalent spectral radiance for 1 ms integration time.

standard deviation of the dark signal and performing radiometric calibration with the radiometric calibration coefficient. It can be used for signal-to-noise ratio (SNR) analysis. The radiometric calibration coefficient for the centre pixel is shown in Fig. 4. The corresponding NESR for an integration time of 1 ms is shown in Fig. 5. The spectral region above 1000 nm is strongly influenced by system noise due to the low quantum efficiency of the CCD-sensor in this region and therefore discarded in further data analysis.

### 3.2 Spectral Calibration

Spectral calibration is needed to successfully derive reflectance spectra or physical parameters of measurement targets. It describes the response of the sensor to discrete light of known wavelength and is used to determine the centre wavelengths and spectral resolution for each spectral channel. The response function of each channel can be approximated with a Gaussian curve, the spectral resolution is defined as the full width half maximum (FWHM) of the function. The peak response of the spectrometer to an infinitesimally narrow emission line describes the centre wavelength of each channel. Special line emission lamps with different gas fills are used to produce narrow, intense lines from the excitation of the gases. Measurements with HgAr-, Xe- and Ne-gas lamps provide emission lines, which cover the whole spectral range of interest. The line width of the emission lines

is much smaller than the spectral resolution of the spectrograph and thus well suited for wavelength calibration (CHEN 1997). Fig. 6 shows the response of the centre channels on the spatial axis to the Xenon lines, in Fig. 7 the 4th order polynomial-fit for the wavelength calibration of the spectral channels is shown. The nominal spectral resolution of the spectrograph is stated as 2.8 nm by the manufacturer. The 1080 spectral pixels of the CCD-Sensor are binned with the factor of 3 which leads to a subset of 331 spectral channels in the 380 nm – 1100 nm region with a spectral sampling interval of approximately 2.2 nm. An Oriel Cornerstone monochromator with a spectral resolution of 0.5 nm is used for sensitivity analysis of adjacent pixels to monochromatic light with 0.1 nm increment. Results of the measurements with line emission lamps and monochromator showed a FWHM between 3.2 nm and 4.7 nm for the binned configuration, depending on the spec-

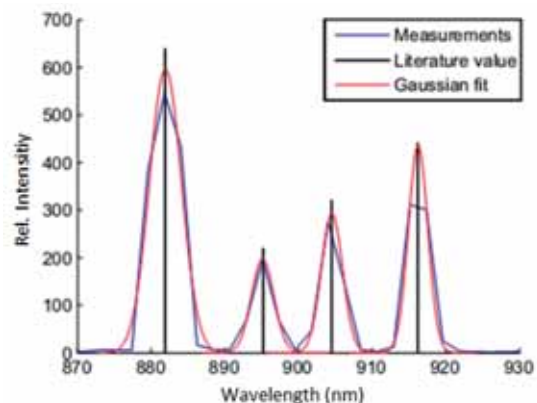


**Fig. 6:** Measurement of Xenon lines.

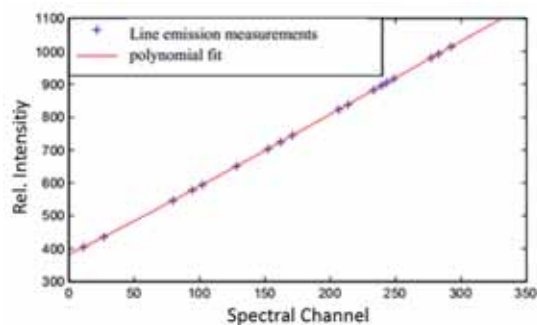


**Fig. 7:** Wavelength calibration with line emission lamps.

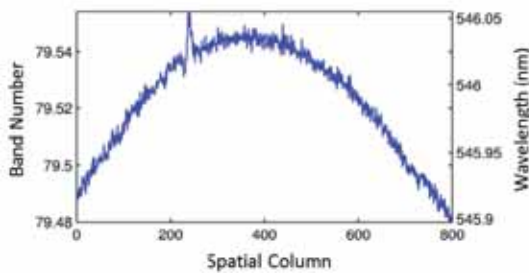


**Fig. 8:** Band position and according wavelength of the 546 nm Hg emission line.

tral channel. In unbinned mode, the FWHM is in the same order of magnitude. Thus, the binning reduces the data volume and increases the SNR without losing spectral information. The bending of spectral lines across the spatial axis (spectral smile) is investigated by comparison of the peak response of all spatial pixels to monochromatic light. Fig. 8 shows a variation of less than 0.1 pixels (3x binned) along the spatial axis for the 546 nm Hg emission line, which is equivalent to 0.2 nm. The bending of spatial lines across spectral axis (keystone) is given by the manufacturer to be smaller than  $5 \mu\text{m}$  which is 0.34 pixels at 2x spatial binning.

### 3.3 Data processing

The results of the laboratory calibration are used for radiometric pre-processing after measurement flights. In a first step, the raw data are corrected for dark signal and can then be converted to spectral radiance by applying the radiometric calibration coefficients. Afterwards, atmospheric distortions have to be corrected. This is done using radiative transfer tools based on the open source software package libRadtran with the core radiative transfer tool uvspec (MAYER & KYLLING 2005). Besides time, date and location, further input-parameters like temperature and humidity are measured during flight time. In addition, a sun-photometer is used to measure the aerosol-optical depth. Based on the spectral calibration of the hyperspectral instrument, a sensor specific wavelength-grid is defined for the numerical calculation of ground and path ra-

diance. As an alternative method, the reflected radiance of a calibrated diffuse grey reference panel with 50% reflectance level can be measured before and after a flight. Reference values are calculated through linear interpolation for the whole flight to derive reflectance values. The linear interpolation method is suitable for stable weather conditions and flight times shorter than 30 minutes (MIURA & HUETE 2009). Finally, geometric rectification and georeferencing have to be performed. Position and attitude of the aircraft are calculated in post-processing with 100 Hz. The beginning and end of each image strip is triggered by the autopilot and marked with a GPS timestamp. A camera-timestamp is stored in every single line-image and used for connecting the images with the position and attitude of the UAS at each exposure. Based on the collinearity equations, custom software was developed for direct georeferencing of the image strips in UTM coordinates on flat terrain or digital elevation model. The correction of boresight angles is implemented with a differential rotation matrix. Final data is stored in ENVI-compatible format and can be further processed with classical remote sensing software packets.

## 4 Results and Discussion

In early 2012, first test flights were performed to prove the system under operational conditions. Parameters like frame rate, exposure time and flight speed were adapted to avoid gaps in image strips. IMU and GPS measurements of the test flights were used for tuning of the Kalman-filter. Tab. 3 shows typical parameters for sensor operation during measurements. In the summer of 2012, the first measurement flights over agricultural test fields were performed. The flight altitude was 300 m above ground. A frame rate of 20 fps and an average ground speed of 15 m/s lead to a ground sampling distance of  $0.5 \text{ m} \times 1 \text{ m}$ . The data were spatially resampled with nearest neighbour method to match a  $1 \text{ m} \times 1 \text{ m}$  UTM grid. Fig. 9 shows an OpenStreetMap aerial photo which is overlaid with a part of a radiometrically calibrated hyperspectral image-strip in RGB-representation.

The hyperspectral image section covers different areas like forest, bare soil or asphalt. As no additional atmospheric measurements were taken on this day, reflectance spectra

**Tab. 3:** Typical parameters for measurement flights.

Flight altitude above ground level	100 m – 300 m
Spatial binning	2x
Spatial pixel	800
FOV/IFOV	1.16 rad/1.45 mrad
Ground sampling distance (GSD)*	0.5 m x 1 m
Swath width*	395 m
Swath length**	1000 m
Spectral binning	3x
Spectral channels	331
Spectral range	380 nm – 1100 nm
Spectral sampling	2.2 nm
Flight time	25 min – 30 min
* valid for 300 m flight altitude	
** limited through line of sight regulation	



**Fig. 9:** Image strip in RGB-representation; map: ©OpenStreetMap.

were calculated based on the reference panel method. Three pre-processed reflectance spectra, which were directly extracted from single pixels of the image in Fig. 9, are shown in Fig. 10. The vegetation reflectance spectrum shows the typical maximum in the green wavelength along with the significant red edge transition zone between visible and near infrared wavelength. These features provide the basis for further investigations like estimation of chlorophyll content, leaf area index or other biophysical parameters (LIU et al. 2004). Also, heterogeneities within one agricultural field are visible and can be utilized for estimating yields or variable-rate application of nitrogen. Reference ground spectra were obtained with an Avantes AvaSpec-128 fibre optic spectrometer for the wavelength region of 500 nm – 1000 nm to prove the spectral image quality. Fig. 11 shows a comparison of UAS and ground measurements for bare soil. The

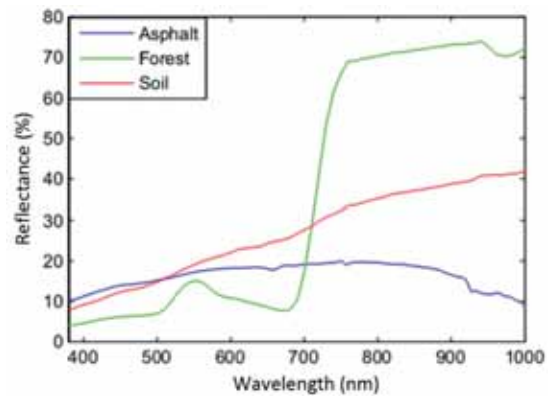


**Fig. 10:** Reflectance spectra for asphalt, forest and soil.

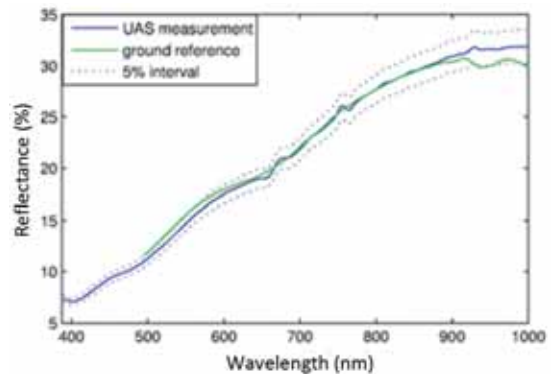


**Fig. 11:** Comparison of ground and airborne measurements of bare soil.

results show a good congruency between both measurements and confirm the high spectral quality of the UAS hyperspectral data. The relative difference between both measurements is smaller than 5%.

The hyperspectral image strip in Fig. 9 was directly georeferenced after post-processing of IMU and GPS data. It can be seen, that there are still geometric distortions which are not corrected properly. Deviations from the aerial image lie in the range of 1 m – 10 m and are particularly noticeable on straight lines like the north-south street between the forest and the field in Fig. 9. The street shows typical S-shaped distortions, which are most likely the result from limited accuracy of the MEMS-sensors. Other studies experienced similar problems with direct georeferencing of line scanner imagery based on lightweight

MEMS sensors (HRUSKA et al. 2012). To increase the accuracy of georeferencing, a new approach is currently adopted. An additional industrial matrix camera, which is triggered synchronously to the line scanner, was integrated in the UAS. It offers the possibility to evaluate very high overlapping images with classical photogrammetric techniques and calculate the exterior orientations of the camera. The orientation can then be used in the direct georeferencing process of the line scanner. Estimations of the Kalman filter are applied as initial values for the exterior orientation of the matrix camera. First tests with the additional camera already show very promising results. Fig. 12 shows a hyperspectral image strip, which is geocorrected based on GPS/IMU measurements (top) and based on exterior orientation of the additional matrix camera (bottom). It can be seen, that geometric distortions are significantly reduced with the integration of the matrix camera. Detailed accuracy assessment of the geometric performance with measurement and analysis of ground control points will be performed in the near future.



**Fig. 12:** Direct georeferencing based on GPS/IMU (top) and exterior camera orientation (bottom).

## 5 Conclusion and Outlook

In this study, we developed a new light-weight hyperspectral sensor system for use on an UAS. The motivation for the study was to enable the recording of high spatial and spectral resolution imagery in the visible and near infrared spectrum, with high temporal flexibility at low operational costs. The system was successfully integrated in the remote sensing platform “Stuttgarter Adler” and showed the ability to acquire spatially detailed and high quality spectral remote sensing data. Based on calibration methods in the laboratory and reference field measurements, a complete processing chain was developed to generate a radiometric and spectral calibrated image. Exemplary reflectance spectra from first measurement flights have been presented in this paper. A comparison with ground measurements confirmed the good spectral performance of the instrument and showed the potential to provide detailed spectral information to scientists and users. Orthorectification methods were implemented for direct geore-

ferencing of the image strips based on post-processing of IMU and GPS measurements. First results indicated geometric distortions after orthorectification in the range of 1 m – 10 m. To increase the geometric accuracy, a new approach for direct georeferencing, including an additional matrix camera, is proposed. A similar approach has been successfully implemented by WALLACE et al. 2012 for direct georeferencing of LIDAR point clouds. For absolute accuracy assessment and bore-sight alignment determination, measurements with ground control points and overlapping flight lines in cross formation have to be performed. In cooperation with the Institute of Crop Science of the University of Hohenheim, hyperspectral remote sensing data shall be used for the determination of spectral characteristics of winter wheat and compared with ground based measurements in the upcoming vegetation period.

## References

- BRISSET, P., 2006: The Paparazzi solution. – European Micro Air Vehicle Conference and Flight Competition, EMAV 2006, Braunschweig.
- BERNI, J., ZARCO-TEJADA, P.J., SUAREZ, L. & FERERES, E., 2009: Thermal and Narrowband Multispectral Remote Sensing for Vegetation Monitoring From an Unmanned Aerial Vehicle. – *IEEE Transactions on Geoscience and Remote Sensing* **47** (3): 722–738.
- CHEN, H., 1997: Remote sensing calibration systems: An introduction. – *Studies on geophysical optics and remote sensing*, A. Deepak Publishing, Hampton, Virginia, USA.
- COCKS, T., JENSSSEN, R., STEWART, A., WILSON, I. & SHIELDS, T., 1998: The HyMap airborne hyperspectral sensor: The system, calibration and performance. – *1st EARSeL Workshop on Imaging Spectrometry*: 37–42.
- GREEN, R.O., EASTWOOD, M.L., SARTURE, C.M., CHRIEN, T.G., ARONSSON, M., CHIPPENDALE, B.J., FAUST, J.A., PAVRI, B.E., CHOVIT, C.J., SOLIS, M., OLAH, M.R. & WILLIAMS, O., 1998: Imaging spectroscopy and the airborne visible/infrared imaging spectrometer AVIRIS. – *Remote Sensing of Environment* **65** (3): 227–248.
- HABOUDANE, D., TREMBLAY, N., MILLER, J. & VIGNEAULT, P., 2008: Remote estimation of crop chlorophyll content using spectral indices derived from hyperspectral data. – *Geoscience and Remote Sensing, IEEE Transactions on* **46** (2): 423–437.
- HRUSKA, R., MITCHELL, J., ANDERSON, M. & GLENN, N.F., 2012: Radiometric and Geometric Analysis of Hyperspectral Imagery Acquired from an Unmanned Aerial Vehicle. – *Remote Sensing* **4** (9): 2736–2752.
- KIRCHGAESSNER, U., 2013: Einsatz eines ferngesteuerten Kleinflugzeugs zur Erfassung von Umweltdaten. – Dissertation, University of Stuttgart.
- KOERNER, F., 2012: Design of a Kalman Filter for Tightly Coupled GPS/INS Integration. – Diploma thesis, University of Stuttgart.
- LIU, J., MILLER, J., HABOUDANE, D. & PATTEY, E., 2004: Exploring the relationship between red edge parameters and crop variables for precision agriculture. – *IEEE International Geoscience and Remote Sensing Symposium* **2**: 1276–1279.
- MAYER, B. & KYLLING, A., 2005: Technical note: The libRadtran software package for radiative transfer calculations – description and examples of use. – *Atmospheric Chemistry and Physics* **5**: 1855–1877.
- MIURA, T. & HUETE, A.R., 2009: Performance of Three Reflectance Calibration Methods for Airborne Hyperspectral Spectrometer Data. – *Sensors* **9** (2): 794–813.
- PUTZE, U., 2013: Auslegung und Instrumentierung eines ferngesteuerten Kleinflugzeugs für die Erdbeobachtung. – Dissertation, University of Stuttgart.
- SCHWARZBACH, M., 2012: Konstruktion und Erprobung eines Bodengerätes zur Messung der BRDF unter natürlichen Beleuchtungsbedingungen. – Dissertation, University of Stuttgart.
- SPECTRAL IMAGING LTD., 2008: ImSpector imaging spectrograph user manual.
- WALLACE, L., LUCIEER, A., WATSON, C. & TURNER, D., 2012: Development of a UAV-LiDAR System with Application to Forest Inventory. – *Remote Sensing* **4** (6): 1519–1543.
- ZARCO-TEJADA, P.J., GONZÁLEZ-DUGO, V. & BERNI, J.A.J., 2012: Fluorescence, temperature and narrow-band indices acquired from a UAV platform for water stress detection using a micro-hyperspectral imager and a thermal camera. – *Remote Sensing of Environment* **117**: 322–337.
- ZARCO-TEJADA, P.J., GUILLÉN-CLIMENT, M.L., HERNÁNDEZ-CLEMENTE, R., CATALINA, A., GONZÁLEZ, M.R. & MARTÍN, P., 2013: Estimating leaf carotenoid content in vineyards using high resolution hyperspectral imagery acquired from an unmanned aerial vehicle (UAV). – *Agricultural and Forest Meteorology* **171–172**: 281–294.

## Addresses of the Authors:

Dipl.-Ing. AXEL BÜTTNER & Prof. Dr. rer. nat. HANS-PETER RÖSER, Universität Stuttgart, Institut für Raumfahrtssysteme, Pfaffenwaldring 29, D-70569 Stuttgart, Tel.: +49-711-685-62056, Fax: +49-711-685-52056, e-mail: {buettner}{roeser}@irs.uni-stuttgart.de

Manuskript eingereicht: Oktober 2013

Angenommen: März 2014